Journal of Physics D: Applied Physics

Buffer optimization for crack-free GaN epitaxial layers grown on Si(1 1 1) substrate by MOCVD

To cite this article: Engin Arslan *et al* 2008 *J. Phys. D: Appl. Phys.* **41** 155317

View the article online for updates and enhancements.

Related content

- Prospects of III-nitride optoelectronics grown on Si
D Zhu, D J Wallis and C J Humphreys
- GaN-based light-emitting diodes on various substrates: a critical review
Guoqiang Li, Wenliang Wang, Weijia Yang et al.
- Structural Properties of GaN Films with AlN Buffer Layers with Varying Growth Temperatures by Plasma-Assisted Molecular Beam Epitaxy
Byoung-Rho Shim, Hideyuki Okita, Kulandaivel Jeganathan et al.

Recent citations

- First observation of electronic trap levels in freestanding GaN crystals extracted from Si substrates by hydride vapour phase epitaxy
Moonsang Lee *et al*
- Microstructural evolution of high quality AlN grown by PAMBE under different growth conditions
Neha Aggarwal *et al*
- Modelling of III-Nitride Epitaxial Layers Grown on Silicon Substrates with Low Dislocation-Densities
Khaled H. Khafagy *et al*

IOP ebooks™

Bringing you innovative digital publishing with leading voices to create your essential collection of books in STEM research.

Start exploring the collection - download the first chapter of every title for free.

This content was downloaded from IP address 193.255.189.6 on 21/08/2019 at 11:18

J. Phys. D: Appl. Phys. **41** (2008) 155317 (10pp) doi:10.1088/0022-3727/41/15/155317

Buffer optimization for crack-free GaN epitaxial layers grown on Si(1 1 1) substrate by MOCVD

Engin Arslan[1,4], Mustafa K Ozturk[2], Ali Teke[3], Suleyman Ozcelik[2] and Ekmel Ozbay[1]

[1] Nanotechnology Research Center–NANOTAM, Department of Physics, Department of Electrical and Electronics Engineering, Bilkent University, 06800 Ankara, Turkey
[2] Department of Physics, Faculty of Science and Arts, Gazi University, Teknikokullar, 06500 Ankara, Turkey
[3] Department of Physics, Faculty of Science and Letters, Balıkesir University, 10145 Balıkesir, Turkey

E-mail: engina@bilkent.edu.tr

Received 14 April 2008, in final form 19 June 2008
Published 18 July 2008
Online at stacks.iop.org/JPhysD/41/155317

Abstract
We report the growth of GaN films on the Si(1 1 1) substrate by metalorganic chemical vapour phase deposition (MOCVD). Different buffer layers were used to investigate their effects on the structural and optical properties of GaN layers. A series of GaN layers were grown on Si(1 1 1) with different buffer layers and buffer thicknesses and were characterized by Nomarski microscopy, atomic force microscopy, high-resolution x-ray diffraction (XRD) and photoluminescence (PL) measurements. We first discuss the optimization of the LT-AlN/HT-AlN/Si(1 1 1) templates and then the optimization of the graded AlGaN intermediate layers. In order to prevent stress relaxation, step-graded AlGaN layers were introduced along with a crack-free GaN layer of thickness exceeding 2.6 μm. The XRD and PL measurements results confirmed that a wurtzite GaN was successfully grown. The resulting GaN film surfaces were flat, mirror-like and crack-free. The mosaic structure in the GaN layers was investigated. With a combination of Williamson–Hall measurements and the fitting of twist angles, it was found that the buffer thickness determines the lateral coherence length, vertical coherence length, as well as the tilt and twist of the mosaic blocks in GaN films. The PL spectra at 8 K show that a strong band edge photoluminescence of GaN on Si (1 1 1) emits light at an energy of 3.449 eV with a full width at half maximum (FWHM) of approximately 16 meV. At room temperature, the peak position and FWHM of this emission become 3.390 eV and 58 meV, respectively. The origin of this peak was attributed to the neutral donor bound exciton. It was found that the optimized total thickness of the AlN and graded AlGaN layers played a very important role in the improvement of quality and in turn reduced the cracks during the growth of GaN/Si(1 1 1) epitaxial layers.

(Some figures in this article are in colour only in the electronic version)

1. Introduction

As a substrate for the growth of GaN/AlGaN epitaxial layers, silicon has many advantages as compared with SiC and sapphire due to its high crystal quality, low cost, good electrical and thermal conductivity and large area size [1–7]. Due to these advantages, gallium nitride growth on Si(1 1 1) wafers has attracted considerable academic and commercial attention. However, because of the large mismatches in the lattice parameter (−16.9%) and thermal expansion coefficients (approximately 57%) between Si and GaN, cracking occurs along the equivalent $\{1\,-1\,0\,0\}$ GaN plane during the cool down [4–11]. Cracking significantly reduces the performance of GaN-based devices due to their current-scattering centres

[4] Author to whom any correspondence should be addressed.

 © 2008 IOP Publishing Ltd Printed in the UK

for light propagation as well as poor crystal quality [2]. The growth conditions and quality of the crystals strongly affect the crack density. The average size of the crack-free surface areas on an epitaxial sample can be increased by manipulating the growth conditions as well as the post-growth heat treatment. However, the appearance of cracks is quite random on the film, which produces critical difficulties in device applications. Therefore, the control of the crack distribution in a large area film is the main issue of this study [3–9].

Many methods have been reported to eliminate the cracks and to improve the crystal quality. Kim *et al* [10] used a five-step graded $Al_xGa_{1-x}N$ ($x = 0.87$–0.07) interlayer between an AlN buffer layer and GaN on Si(1 1 1). An AlGaN/GaN superlattice was used by Nikishin *et al* [4] instead of an AlGaN layer, and the insertion of a low-temperature AlN (LT-AlN) interlayer into the bulk high growth temperature GaN was reported by Amano *et al* [8]. However, because of the excessively large thermal expansion coefficient mismatch, these methods have not achieved a perfect crack-free GaN/Si(1 1 1) epitaxy when compared with the growth of GaN on the sapphire substrate.

The insertion of a low-temperature AlN (LT-AlN) interlayer into the bulk high growth temperature GaN, which was proposed by Amano *et al* [8], is considered to be a promising approach to the elimination of cracks for GaN growth on Si(1 1 1) substrates. The LT-AlN interlayer can lead to a lower threading dislocation (TD) density, improvement of the crystalline quality and the reduction of tensile stress and cracking that is generated during the high-temperature GaN growth or cooling [12–14, 16]. The AlN epitaxial layers are widely applied as nucleation layers (NLs) for GaN growth on silicon and serve not only as wetting layers for GaN but also as barrier layers to prevent Ga meltback etching.

Graded AlGaN intermediate layers between the AlN NL and the GaN introduce compressive stress during growth in order to compensate for the tensile stress that is generated primarily during the cool down from the growth temperature [11]. The growth of a successive $Al_xGa_{1-x}N$ layer introduces compressive stress when $x < y$ due to the negative lattice mismatch between GaN and AlN according to [10, 13].

The influence of the growth parameters, including the growth temperature, V/III ratio and thickness, has been studied in terms of the crystalline quality of the top GaN layers. However, there have been very few reports on the optimization of HT-AlN and the step-graded AlGaN layers relating the crystalline quality, surface morphology and stress in the epitaxial GaN layers [11, 13].

In this paper, we demonstrate extremely smooth and flat GaN high-quality and nearly crack-free GaN/Si(1 1 1) epitaxy. We also discuss the effects of the LT-AlN and HT-AlN template layers' thicknesses. We investigated the changes in morphologies as a function of the HT-AlN layer thickness. As a next step, the step-graded AlGaN intermediate layers were successfully introduced between the AlN NL and GaN to prevent the cracking of GaN. Then the thickness of the step-graded AlGaN intermediate layers was optimized. We have investigated in detail the effects of the LT-AlN and HT-AlN template layers' thicknesses on the characteristics of the structural features (correlation lengths normal and parallel to the substrate surface, tilt and twist, heterogeneous strain) and dislocation densities (edge and screw types) by HXRD and the optical properties by temperature-dependent PL measurements of the hexagonal epitaxial GaN films grown on Si (1 1 1).

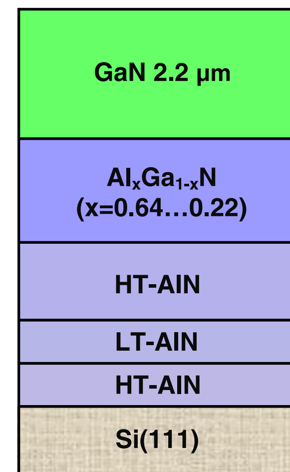

Figure 1. Schematic view of GaN/Si(1 1 1) with the HT-AlN/LT-AlN/HT-AlN/$Al_xGa_{1-x}N$ buffer system.

2. Experimental procedure

GaN epitaxial layers on the Si substrate were grown in a low-pressure metalorganic vapour phase deposition (MOCVD) reactor (Aixtron 200/4 HT-S), using trimethylgallium (TMGa), trimethylaluminum (TMAl) and ammonia as Ga, Al and N precursors, respectively. H_2 was used as a carrier gas during AlN and AlGaN growth. Before loading the substrates, Si substrates were sequentially degreased by $H_2OSO_4 : H_2O_2 : H_2O$ (2 : 1 : 1) solutions for 1 min and etched in a 2% HF solution for 1 min, rinsed in de-ionized water and dried with a nitrogen gun.

At the beginning of the growth of AlN, the substrate was baked in an H_2 ambient at 1100 °C for 20 min to remove the native oxide. For all the samples, in order to prevent the formation of the amorphous SiN_x layer, we carried out Al predeposition on the silicon surface. The buffer structures included low-temperature (700 °C) AlN (LT-AlN) layers, high-temperature (1100 °C) AlN (HT-AlN) layers and a five-step graded $Al_xGa_{1-x}N$ interlayer ($x = 0.64$, 0.54, 0.40, 0.33, 0.22). In all the samples, the GaN layers were grown at 1050 °C. The AlN template layer growth temperature produces the best crystalline quality and a reasonably low tensile stress in the layer.

Five GaN samples were grown using different buffer structures (figure 1). The structure of sample A is Si(1 1 1)/30 nm HT-AlN/30 nm LT-AlN/300 nm HT-AlN/$Al_xGa_{1-x}N$/GaN. In samples B and C, we used the same buffer structures and changed the HT-AlN layer thickness to 400 nm and 500 nm, respectively. In all three samples, we used a 700 nm $Al_xGa_{1-x}N$ interlayer ($x = 0.64$, 0.54, 0.40, 0.33, 0.22) with different layer thicknesses. The AlGaN layer's thickness ratio was approximately: 1/1.5/2/2.5/3. In samples

D and E, Si(1 1 1)/30 nm HT-AlN/30 nm LT-AlN/400 nm HT-AlN/$Al_xGa_{1-x}N$/GaN structures were grown. In these samples the $Al_xGa_{1-x}N$ interlayer thicknesses changed to 800 nm and 950 nm, respectively. In this study, five different samples were grown with different buffer systems: samples A, B, C, D and E with buffer systems 30 nm HT-AlN/30 nm LT-AlN/300 nm HT-AlN/700 nm $Al_xGa_{1-x}N$, 30 nm HT-AlN/30 nm LT-AlN/400 nm HT-AlN/700 $Al_xGa_{1-x}N$, 30 nm HT-AlN/30 nm LT-AlN/500 nm HT-AlN/700 nm $Al_xGa_{1-x}N$, AlN/30 nm LT-AlN/400 nm HT-AlN/800 nm $Al_xGa_{1-x}N$ and AlN/30 nm LT-AlN/400 nm HT-AlN/950 nm $Al_xGa_{1-x}N$, respectively.

The crystalline quality of the GaN layers was examined by high-resolution x-ray diffraction (HRXRD). The x-ray diffraction (XRD) was performed using a Bruker D-8 high-resolution diffractometer system, delivering Cu Kα1 (1.540 Å) radiation, using a prodded mirror and a 4-bounce Ge(2 2 0) symmetric monochromator. Data were collected on the (0 0 0 2), (0 0 0 4), (0 0 0 6), (1 0 −1 5), (2 0 −2 2), (1 2 −3 1), (1 0 −1 1), (1 0 −1 3) and (1 1 −2 4) reflections only with ω and $\omega - 2\theta$ scans. PL measurements were carried out in the temperature range 8–300 K with the sample placed in a closed-cycle cryostat. A 325 nm He–Cd laser with 30 mW optical power was used as an excitation source. The luminescence was collected by suitable lenses and then dispersed with a 550 mm spectrometer and detected by CCD. The surface morphology was characterized by Nomarski interface contrast optical microscopy and atomic force microscopy (AFM).

3. Results and discussion

We used AlN layers in order to grow III-nitrides on Si(1 1 1) surfaces [17]. In order to minimize the disorientation of GaN islands on top, a smooth surface of AlN is required. In our study, we used an HT-AlN interlayer with thicknesses ranging from 300, 400 to 500 nm. The crystalline quality, which was characterized by HRXRD, improves and more stress relaxation is achieved when the HT-AlN interlayer possesses thicknesses exceeding 400 nm. The growth of AlN epitaxial layers starts with Volmer–Weber island growth due to the large lattice mismatch between AlN and the silicon substrate (−17%) [18]. As the thickness of the AlN epitaxial layer increases, the island density is reduced and the size of the islands becomes increasingly larger. When the thickness of the AlN layer reaches 400 nm, the surface is nearly smooth and coalesced, which can be then used as a good template for further AlGaN or GaN growth.

Although the AlN/Si(1 1 1) template was optimized and a rather low tensile stress in the GaN layer was achieved, the GaN layer still suffered from cracking problems. In order to avoid compressive stress relaxation, seven layers of AlGaN with different compositions were introduced, i.e. the Al content was varied in steps. These incremental steps only led to modest changes in the lattice constant. Therefore, we expected to maintain a pseudo-2D growth mode for each successive layer. This in turn led to a smooth and crack-free GaN surface, as shown in figure 2. We found an optimal value for the total thickness of the step-graded AlGaN intermediate layers. This was achieved by varying the total thickness of these intermediate layers from 700 to 950 nm while keeping the thickness ratio constant.

The surface morphologies of all the samples were studied by optical Nomarski interference microscopy. Figures 2(*a*)–(*d*) show the Nomarski microscopy (NM) photographs of samples A, B, C, D and E. The variation of the cracks in the samples grown under different conditions is clearly revealed. A nearly crack-free surface was achieved on sample B with a 700 nm AlGaN graded interlayer and 400 nm HT-AlN layers GaN grown on the silicon substrate. This indicates that the cracks of GaN on Si are seriously affected by the thickness of the AlN and AlGaN buffer.

The measured crack densities for samples A, B, C, D and E were about 15/cm, 4/cm, 9/cm, 22/cm and 28/cm, respectively. In our case, the crack density increased for those samples with less than 300 nm HT-AlN thickness. It also increased above 500 nm. In our study, we obtained a completely crack-free 1.9 μm GaN layer with a 30 nm HT-AlN/30 nm LT-AlN/400 nm HT-AlN/700 nm graded $Al_xGa_{1-x}N$ buffer system. The cracks along {1 −1 0 0} in the GaN layers grown on the Si substrate have been reported by many groups [10, 19]. Cracks in GaN on Si are known to be formed during the cooling stage due to a large tensile stress that is caused by the large difference in the thermal expansion coefficients [13–15].

The surface morphology of the GaN layer grown on the step-graded AlGaN intermediate layers is extremely smooth. The root-mean-square (RMS) roughness and the maximum peak-to-valley roughness are between 0.4 and 0.7 nm. Figures 3(*a*)–(*e*) show a comparison of the surface morphology for samples A, B, C, D and E, respectively. Sample B has a smooth surface with a low rms roughness (rms = 0.4 nm) compared with samples A, C, D and E. Sample B with a 700 nm graded AlGaN interlayer shows fewer defects, but sample E with a 950 nm graded AlGaN interlayer shows structural defects along with a rough morphology, in which similar surface defects have been associated with open core dislocations that have a screw-type component [9, 13, 43–46].

XRD was performed for all the samples to investigate the crystal phase of the GaN on Si(1 1 1). Figure 4 shows the θ scan XRD pattern of a GaN layer grown on a HT-AlN and graded $Al_xGa_{1-x}N$ interlayer buffer system. The diffraction patterns exhibited only the dominant wurtzite GaN crystalline (0 0 0 2), (0 0 0 4) and (0 0 0 6) peaks plus two peaks from the Si substrate and a small peak from the AlN buffer layers. For sample B, the (0 0 0 2), (0 0 0 4) and (0 0 0 6) reflections of wurtzite GaN are clearly observed at 34.56°, 73.02° and 126.24°, respectively. These results indicate a grown GaN layer with the normal orientation along the *c*-axis of wurtzite crystalline structures [9].

An in-plane Φ scan was also taken by rotating the sample around its surface-normal direction to investigate the in-plane alignment of the GaN film. Figure 5 shows the Φ scan pattern of the (1 0 −1 1) plane of sample B. It can be seen in figure 5 that diffraction peaks from the (1 0 −1 1) plane of GaN were observed at 60° intervals, confirming the hexagonal structure of the GaN epilayer.

Heteroepitaxial thin films having a large lattice mismatch with respect to the substrate form a mosaic structure of slightly

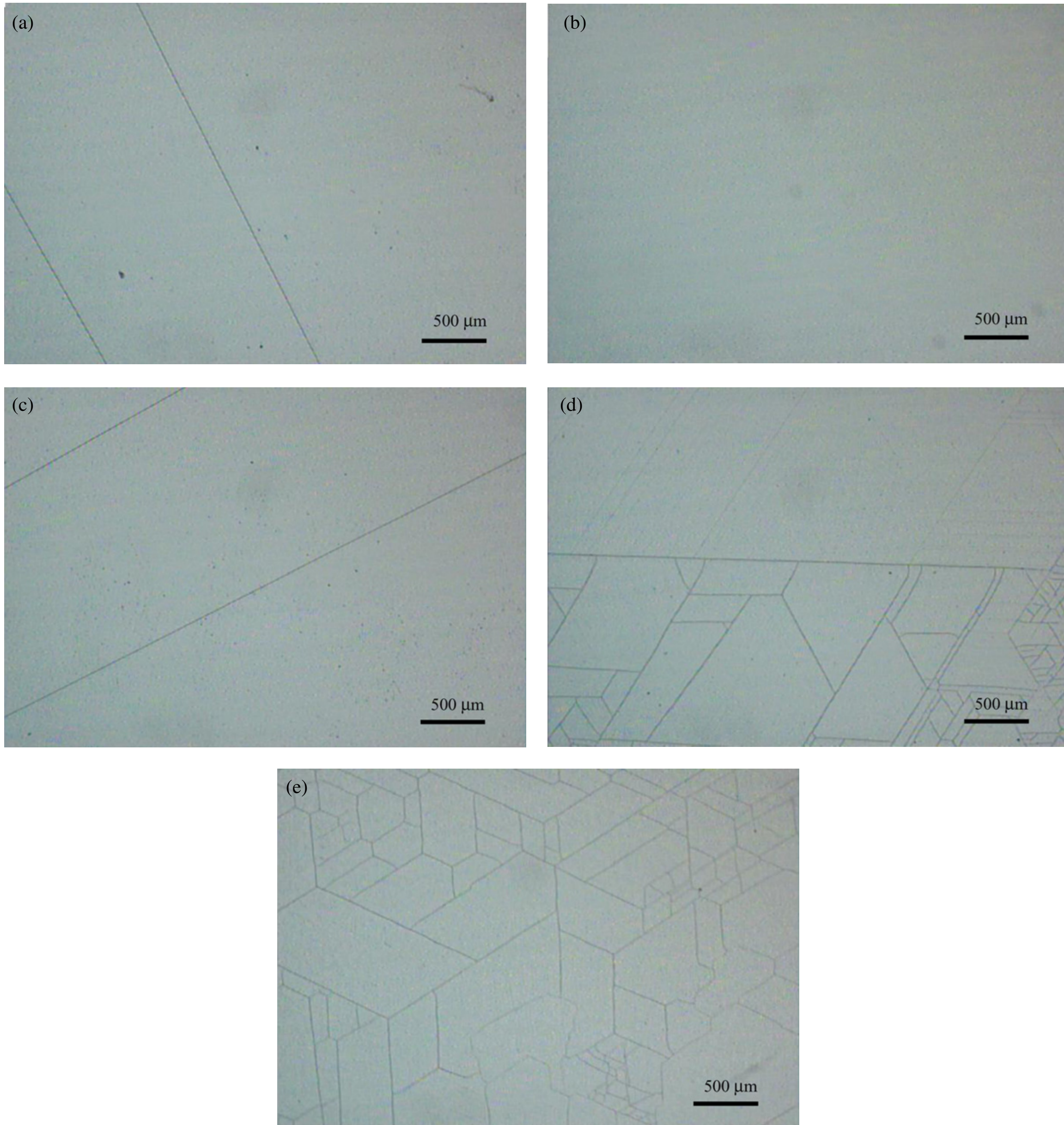

Figure 2. Optical Nomarski microscopy views of (*a*) sample A, (*b*) sample B, (*c*) sample C, (*d*) sample D and (*e*) sample E.

misoriented sub-grains [20, 21, 23, 24], which is characterized by the nucleation of slightly misoriented islands and the coalescence of these islands towards a smooth surface. The mosaic structure of the epilayers is determined by the size and angular distribution of the mosaic blocks. The vertical and lateral correlation lengths, heterogeneous strain and degree of mosaicity expressed by the tilt and twist angles are important parameters in characterizing the quality of the epitaxial films with a large lattice mismatch to the substrate [20, 22, 25]. The mosaic blocks are assumed to be slightly misoriented with respect to each other. The out-of-plane rotation of the blocks perpendicular to the surface normal is the mosaic tilt, and the in-plane rotation around the surface normal is the mosaic twist. The average absolute values of the tilt and twist are directly related to the full width at half maximum (FWHM) of the corresponding distributions of crystallographic orientations [24, 25].

The parameters, vertical and lateral coherence length and tilt angle can be obtained from the Williamson–Hall measurement and the twist angle from an approach that was developed by Srikant *et al* [25] or from a direct measurement [26], which explains the superposed effect of tilt and twist on the broadening of the FWHMs of off-axis plane rocking curves [27].

Each contribution to the broadening of particular XRD curves can be separated in a Williamson–Hall measurement [20, 27]. Specifically, in triple-axis diffractometer measurements, the broadening of the rocking curve (angular-scan or ω scan) of the symmetric (0 0 0 2), (0 0 0 4) and (0 0 0 6) reflections for the GaN epitaxial layer is influenced only by the tilt angle α_{tilt} and the short coherence length parallel to the substrate surface $L_{\parallel}$.

Separation analogous to the tilt angle α_{tilt} and short coherence length can be made with a Williamson–Hall

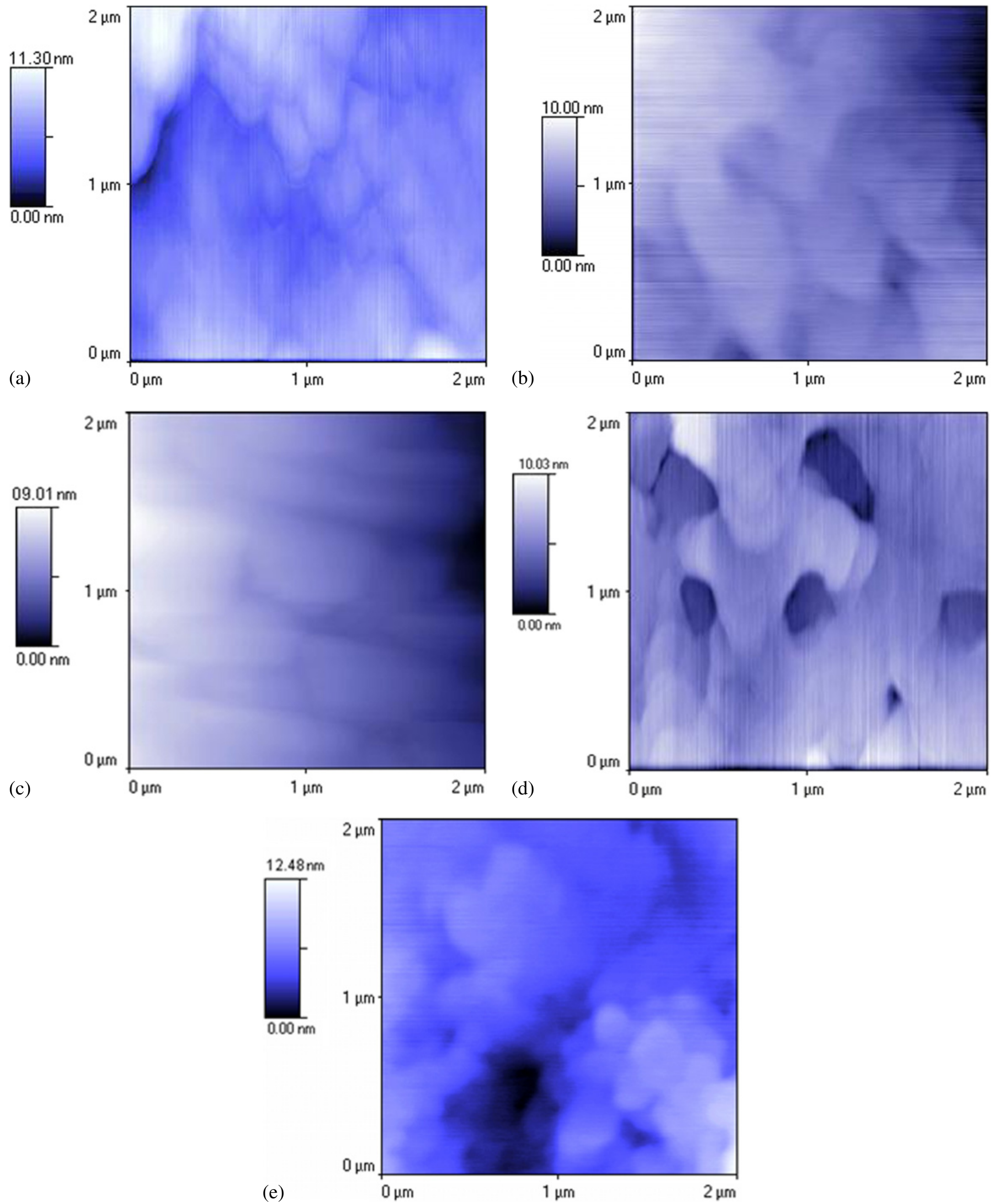

Figure 3. AFM images (2 μm $\times$ 2 μm scans) of GaN films in (*a*) sample A, (*b*) sample B, (*c*) sample C, (*d*) sample D and (*e*) sample E.

plot, when $\beta_\omega(\sin\theta)/\lambda$ is plotted against $(\sin\theta)/\lambda$ for each reflection and fitted by a straight line. Then the tilt angle α_{tilt} is obtained from the slope of the linear dependence and the lateral coherence length $L_\parallel$ ($L_\parallel = 0.9/(2y_0)$) from the inverse of the y-intersection y_0 of the fitted line with the ordinate, where β_ω is the FWHM in angular units, θ is the Bragg reflection angle and λ is the x-ray wavelength.

In the radial-scan direction ($\omega-2\theta$ scan) of the symmetric reflections (0 0 0 2), (0 0 0 4) and (0 0 0 6), a small vertical correlation length and a heterogeneous strain along the c-axis cause a broadening of the Bragg reflections. These two parameters $L_\perp$ and $\varepsilon_\perp$ can similarly be derived from the Williamson–Hall plot. In the Williamson–Hall plot, $\beta_{\omega-2\theta}(\cos\theta)/\lambda$ is plotted against $(\sin\theta)/\lambda$ for each reflection and again fitted by a straight line. From the y-intersection y_0 the vertical correlation length $L_\perp$ can be calculated ($L_\parallel = 0.9/(2y_0)$) and the heterogeneous strain $\varepsilon_\perp$ can be estimated directly from the slope of the line which is $4\varepsilon_\perp$.

Figure 6 shows the corresponding Williamson–Hall plots for reflections (0 0 0 2), (0 0 0 4) and (0 0 0 6) for triple-axis (*a*) ω scan and (*b*) $\omega-2\theta$ of all the samples with a different buffer system. The straight lines are linear fits of the experimental data. The expected linear behaviour of the graphs

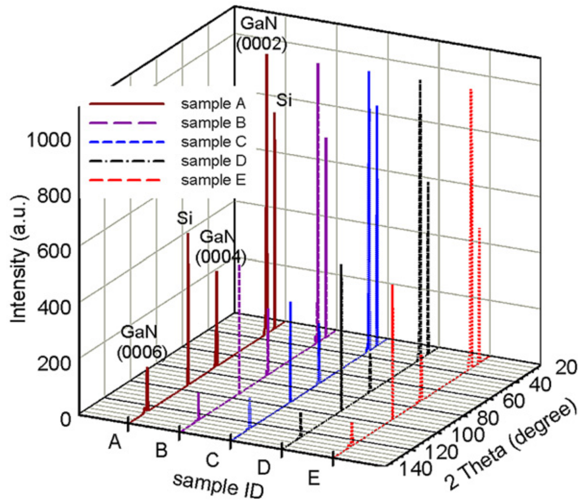

Figure 4. The XRD pattern of all the samples.

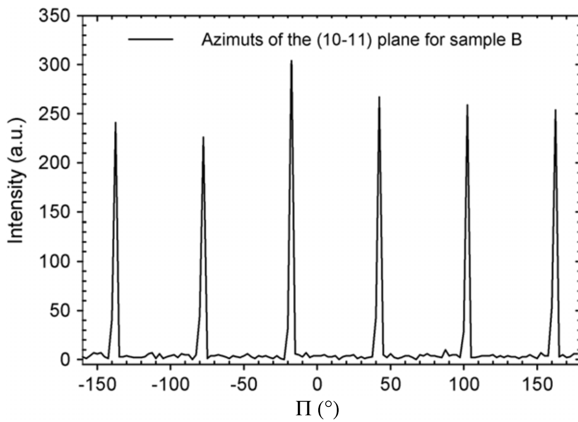

Figure 5. Phi scan curve of an asymmetric GaN (1 0 −1 1) reflection plane for sample B. Every peak shows azimuths of the (1 0 −1 1) plane. The diffractive peak repeats every 60°.

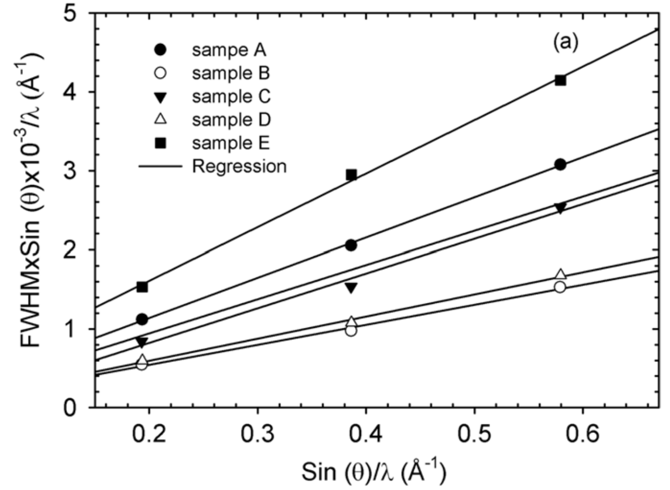

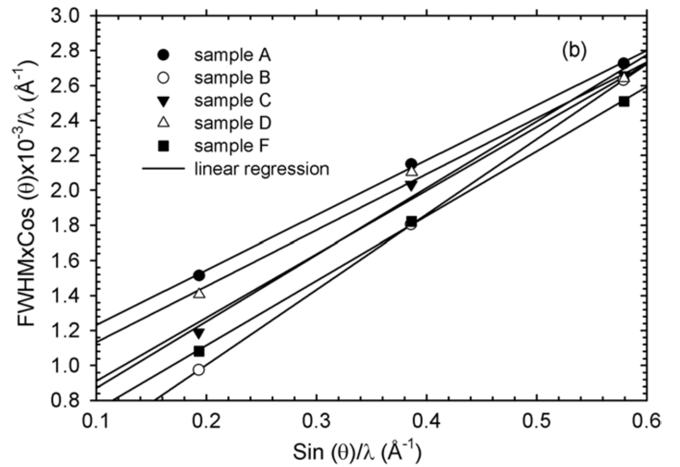

Figure 6. Williamson–Hall plot for GaN layers for all samples. (*a*) Triple-axis ω scan and (*b*) triple-axis $\omega - 2\theta$ scan were measured for the (0 0 0 l) ($l = 2, 4, 6$) reflections indicated in the figure. The lines result from a linear fit of the data.

is experimentally well confirmed, which gives rather accurate tilt angle values.

The lateral coherence lengths $L_{\parallel}$ and tilt angles are shown in table 1. As can be clearly seen, the tilt angles for all the samples were rather small. It can be seen from this table that minimum tilt angle values were obtained for sample B with a 400 nm HT-AlN layer and a 700 nm AlGaN layer. Furthermore, the same tilt angle values can be obtained for sample D with an 800 nm AlGaN buffer layer. The lateral coherence lengths were determined to range from 176 to 1500 nm. As seen in table 1, the maximum values were observed for sample B.

The vertical coherence lengths $L_{\perp}$ values are shown in table 1. The values range from 500 to 1800 nm. For sample B, the maximum $L_{\perp}$ value was 1800 nm.

The strain normal to the substrate $\varepsilon_{\perp}$ values obtained for all the samples is shown in table 1. The $\varepsilon_{\perp}$ values range from 8.0×10^{-4} to 9.7×10^{-4}. Small changes were observed for a heterogeneous strain with the buffer system thickness.

The mean twist angle between the sub-grains can be extrapolated from a fit to the measured double-axis scans data for different (*hkl*) reflections in a skew symmetric diffraction. Several extrapolation methods have been reported in the literature for a mean twist angle calculation [20, 25, 28]. However, all these methods include a complicated calculation and fitting procedure for the extraction of the twist angle from the experimental data. On the other hand, Zheng *et al* [26] proposed a simple empirical approach to obtain the mean twist angle directly without falling into complications.

The FWHM of the rocking curve of an imperfect film is composed of several contributions, such as the mean tilt, twist, the average size of the sub-grains and the inhomogeneous strain distributions. Although the broadening, due to a limited domain size and inhomogeneous strain, can be significant in highly imperfect films, their effects have been eliminated by using a slit of 0.6 mm that is placed in front of the detector in double-axis ω scans. Indeed, their contribution to the overall broadening was found to be of minor influence in this measurement case.

In addition, the (0 0 0 2) reflection and (*hkl*) reflections with either h or k nonzero orientation of our samples with triple-axis $\omega - 2\theta$ scans exhibit a small FWHM. The last important point is that the intrinsic width of the reflection for the crystal and the apparatus broadening for all the

Table 1. The properties of the GaN layers that were grown with different interlayers are listed. The second and third columns show the HT-AlN and graded AlGaN layer thickness (nm). In the third and fourth columns, the peak position and the FWHM (meV) of the band emission of PL at room temperature are listed. The buffer layer thickness and structural characteristics of all the samples are given, including the vertical grain size $L_\perp$, lateral grain size $L_\parallel$, vertical heterogeneous strain $\varepsilon_\perp$ parallel to the lattice vector and tilt angle α_{tilt}. The last column shows the rms surface roughness (nm) measured for a 2 × 2 μm^2 scan area.

Sample ID	HT-AlN layer thickness (nm)	AlGaN layer thickness (nm)	PL peak position (eV)	FWHM of PL (meV)	Twist angle (deg)	Tilt angle (deg)	$L_\parallel$ (nm)	$L_\perp$ (nm)	Heterogeneous strain $\varepsilon_\perp(\times 10^{-4})$	Rms roughness (nm)
A	300	700	3.387	62	1.089	0.005	377	500	8.7	0.6
B	400	700	3.390	58	0.468	0.003	1500	2500	9.7	0.4
C	500	700	3.394	67	0.980	0.004	818	900	8.5	0.5
D	400	800	3.389	65	0.746	0.003	1250	562	8.0	0.7
E	400	950	3.396	68	1.363	0.008	176	1125	9.2	0.6

experimental reflections are negligible because these effects amount to only a few arcsec. For this reason, we can only measure the broadening that was caused by the twist using (*hkl*) reflections in skew geometry.

The extended FWHMs of ω and Φ scans were obtained by using the fit of pseudo-Voigt function to the rocking curves. The FWHM of the ω scan increases with the increment of χ, while the FWHM of Φ scan decreases with the increment of χ [26]. They become closer when the (1 2 −3 1) reflection yields χ at 78.6°. These results showed that the rocking-curve widths of ω or Φ scans for this higher χ angle are close to the twist angles. In every respect, the FWHMs of Φ scans are larger than those of χ scans with the change in the inclination angle χ. Therefore, the mean twist angles must be the average value of the FWHMs of ω and Φ scans of $\chi = 78.6°$.

The measured mean twist angle of the GaN layers is shown in table 1. The mean twist angles change with the HT-ALN layer thickness and the AlGaN layer thickness. The minimum mean twist angle value was obtained as 0.468° for sample B. The sample HT-AlN layer thickness was 400 nm and the AlGaN buffer layer thickness was 700 nm. Based on this observation, it can be argued that the mean twist angle of the GaN epilayers grown on the Si substrate is strongly affected by the HT-AlN layer thickness and the AlGaN layer thickness.

It is well known that the GaN epilayers grown on Si(1 1 1) in two steps exhibit a high dislocation density [1–7]. There are three main types of dislocations present in the GaN thin film [20,26,29]: the pure edge dislocation with Burgers vector $b = \frac{1}{3}\langle 1\,1\,\bar{2}\,0\rangle$ ($\langle a\rangle$), the pure screw dislocation with Burgers vector $b = \langle 0\,0\,0\,1\rangle$ ($\langle c\rangle$) and the mixed dislocation with $b = \frac{1}{3}\langle 1\,1\,\bar{2}\,3\rangle$ ($\langle c+a\rangle$). The dislocation density D_{dis} of GaN films can be calculated from the equations [30,31]

$$D_{screw} = \frac{\beta^2_{(0\,0\,0\,2)}}{9b^2_{screw}}, \qquad D_{edge} = \frac{\beta^2_{(1\,0\,1\,2)}}{9b^2_{edge}}, \qquad (1)$$

$$D_{dis} = D_{screw} + D_{edge}, \qquad (2)$$

where D_{screw} is the screw dislocation density, D_{edge} is the edge dislocation density, β is the FWHM measured by XRD rocking curves and b is the Burgers vector length ($b_{screw} = 0.5185$ nm, $b_{edge} = 0.3189$ nm).

Figure 7 shows the edge, screw and total dislocation densities for different samples. As seen in this figure, the edge and screw dislocation densities changed with the HT-AlN layer thickness and the AlGaN intermediate layer thickness. It can be seen that for sample B, with a 400 nm HT-AlN template layer and a 700 nm AlGaN intermediate layer thickness, minimum dislocation densities were obtained.

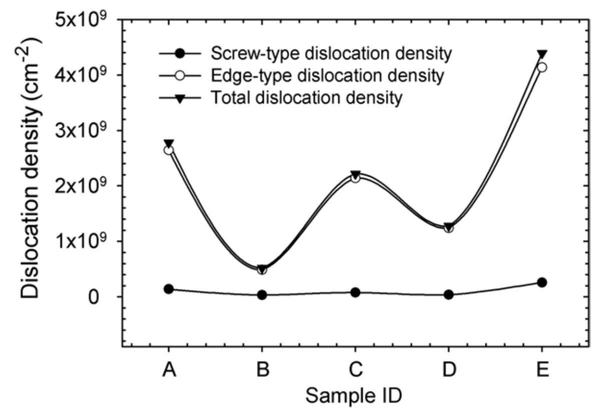

Figure 7. The edge, screw and total dislocation densities for different samples.

The photoluminescence (PL) spectra at room temperature for all the samples were measured. The PL peak and FWHM values for the five samples are all listed in table 1. The samples show a strong PL emission band between 3.387 and 3.394 eV due to the near-band edge emission from wurtzite GaN. The FWHMs of the band edge emission were within the range 58–62 meV. The small FWHM values of the PL emission peaks also indicate a high-quality w-GaN material.

In table 1, the FWHM of the near-band edge emission peak was 58 meV for sample B. It indicates that sample B that was grown with a 700 nm AlGaN layer and a 400 nm HT-AlN layer has the best optical property versus other samples. These results were compared with the result achieved for GaN/Si epilayers [30–32]. The low FWHM values in our films may likely be attributed to the high degree of crystallographic alignment of the buffer layers and to the layers without a grain structure. Jang *et al* [15] used various $Al_{0.3}Ga_{0.7}N$/GaN superlattices as an intermediate layer for GaN/Si(1 1 1) epitaxial layers, in which their reported values for the FWHM values were 34.49 meV.

Figure 8 shows the evolution of PL spectra for sample B over the temperature range 8–300 K. As seen in the figure, the

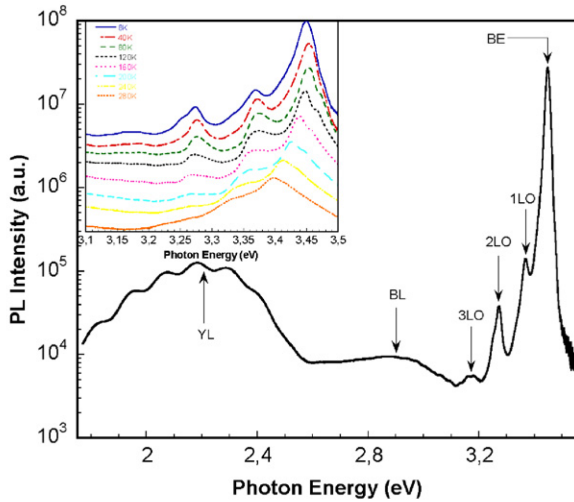

Figure 8. The temperature dependence of the PL spectra and assignment of the peaks for sample B.

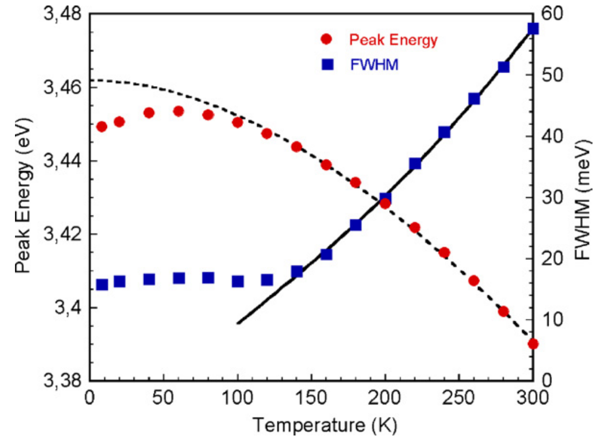

Figure 9. The temperature induced a shift in the energy peak positions of GaN band edge emission together with its FWHM deduced by using Gaussian fits to the PL spectra shown in figure 8. The dashed line and the full circles are drawn by using Varshni's equation (equation (3)) and the solid line is drawn using equation (4).

PL spectra at 8 K were dominated by a GaN band edge emission centred at 3.449 eV and its phonon replicas were separated by approximately 92 meV in successive order. The FWHM of this main peak is approximately 16 meV. At room temperature, the peak position and FWHM of this emission become 3.390 eV and 58 meV, respectively. The origin of this peak was attributed to the neutral donor bound exciton. These types of transitions are commonly responsible for the dominant PL line in undoped and n-type GaN grown by any technique on any substrate. In high-quality strain-free GaN samples with a low concentration of defects, two or more sharp lines that were observed around 3.471 eV were attributed to different neutral shallow donor bound exciton transitions [32,33]. In our case, the energy peak position of the main peak redshifted by approximately 18 meV compared with a strain-free GaN template, which implies that there is a strong tensile stress present in GaN epilayers grown on Si(1 1 1). The shoulder at approximately 3.477 eV, which becomes clearer as the temperature increases (see the inset of figure 8), was attributed to the A-free exciton transition [34,35]. Additional defect-related weak blue luminescence (BL) and strong yellow luminescence (YL) peaks at 2.9 eV and 2.2 eV, respectively, were also observed at the low energy side of the PL spectra at 8 K. The YL was attributed to a shallow donor–deep acceptor transition [36]. The deep acceptor is believed to be the native gallium vacancy (V_{Ga}), while the shallow donor is attributed to substitutional oxygen (O_N) and silicon (Si_{Ga}) or C impurities substituted for the nearest neighbour of the Ga sites [37, 38]. In our case, V_{Ga}–Si_{Ga} complexes are believed to be the main cause of the YL band due to the diffusion of Si impurities from the substrate during growth. The BL band peak at approximately 2.9 eV in GaN was similar to the notorious YL in this material. The BL band is often observed in undoped, Mg- and Zn-doped GaN with a very similar shape and position [36]. The origin of this peak is not clear in our case, but most probably it is due to the transitions from a deep donor to the Mg_{Ga} shallow acceptor arising from the residual memory effect of the MOCVD system.

Figure 9 shows the temperature-dependent PL peak positions and FWHM deduced by applying the Gaussian fit to the experimental data. The temperature dependence of the peak positions of the GaN band edge emission can be fitted by using Varshni's equation;

$$E_g(T) = E_g(0) - \frac{\alpha T^2}{\beta + T}, \qquad (3)$$

where $E_g(T)$ is the transition energy at temperature T, $E_g(0)$ the corresponding energy at 0 K and α and β are known as Varshni's thermal coefficient and Debye temperature, respectively. The best fitted values of α and β are 0.92 meV K^{-1} and 867 K, respectively. These values are similar to those reported by Calle *et al* [34] for the free exciton transition of GaN grown on the Si (1 1 1) substrate. As seen in the figure, although the energy peak position of the band edge emission line follows the typical temperature dependence of the energy gap shrinkage over 80 K, it deviates from Varshni's equation at low temperatures. As the temperature increases from 8 to 80 K, the peak energy blueshifts by approximately 6 meV. This blueshift in the peak position can be interpreted by considering the thermal dissociation of the main bound exciton to other shallower donor bound excitons, which could not be resolved due to the limited linewidth of the PL spectrum. Similar behaviour was also observed by Zhang *et al* [39]. The thermal dissociation of the main bound exciton to free excitons and other shallower donor bound excitons is also accompanied by a change in the relative intensities of these transitions with increasing temperature [40].

Figure 9 also shows the temperature dependence of the FWHM of the main peak. A study of the linewidth of excitons provides information about the scattering mechanisms [41]. Temperature-independent inhomogeneous and homogeneous broadening mechanisms related to various scattering processes such as phonons or excitons can be considered for the observed behaviour of the linewidth. Since the excitation power density of the current measurements is approximately 5 mW cm^{-2} the exciton–exciton interaction can be ignored. If we assume that the linewidth is mainly related to the exciton broadening through phonon scattering, it can be described by

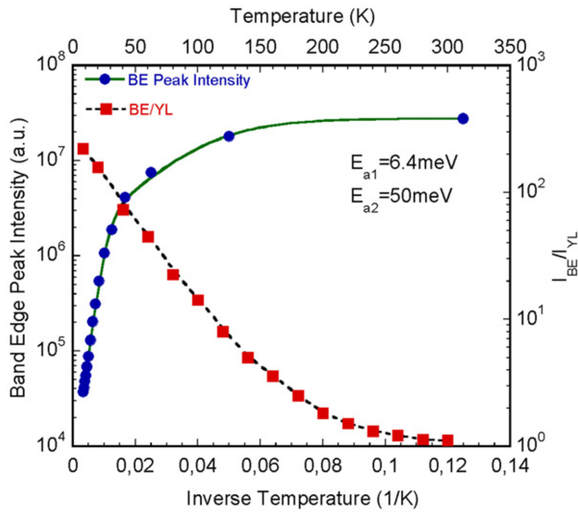

Figure 10. GaN band edge related PL intensity as a function of inverse temperature and the temperature dependence of the relative intensities (I_{BE}/I_{YL}). The solid line is drawn to calculate the activation energies by using equation (5). The dashed line represents the exponential fit to the temperature behaviour of the I_{BE}/I_{YL} ratio.

the expression [41]

$$\mathrm{FWHM}(T) = \Gamma_I + \Gamma_H = \Gamma_I + \gamma_{ac}T + \frac{\Gamma_{LO}}{\exp(-\hbar\omega_{LO}/kT) - 1}, \quad (4)$$

where subscripts I and H refer to inhomogeneous and homogeneous broadening and γ_{ac} and Γ_{LO} are parameters describing the exciton–phonon interactions. It is clearly observed that the FWHM increases with temperature at two different rates. At low temperatures homogeneous broadening is determined by the scattering of excitons by acoustic phonons, which shows a monotonic increase in the FWHM. At high temperatures the exciton–LO phonon interaction becomes the dominant mechanism since the density of LO phonons increases as the temperature increases. Indeed, fitting the experimental data using equation (4) above the temperature of 120 K gives an excellent correlation indicating that the main contribution to the observed FWHM is the exciton–phonon interaction.

Figure 10 shows an Arrhenius plot of the PL intensity for band edge emission over the temperature ranges under investigation. As shown in the figure, the PL intensity of the emission decreases as the temperature increases. The dominant mechanism leading to this thermal quenching of PL intensity is due to the increase in the effects of the nonradiative recombination centres with temperature. As seen in the figure, the PL intensity decreases rather little at low temperatures but decreases more rapidly at high temperatures. This suggests that there are two different mechanisms that are responsible in the low- and high-temperature regimes. The activation energies in these thermally activated processes were calculated using the following equation [42]:

$$I(T) = \frac{I_0}{1 + \sum_{i=1} \alpha_i \exp\left(-\frac{E_{ai}}{k_B T}\right)}, \quad (5)$$

where E_{ai} is the activation energy of the corresponding nonradiative recombination centres, α_i is the process rate parameter and k_B is Boltzmann's constant. The fitted curve is shown as the solid line in figure 10. The thermal activation energies of 6 meV for the low-temperature and 50 meV for the high-temperature regimes were deduced from the best fit by considering the bi-exponential function. At low temperatures, the thermal quenching of the PL peak intensity with 6 meV activation energy could be related to the thermal dissociation of the main donor bound exciton line at 3.449 nm into other shallower donors as discussed in the temperature dependence of the emission peak. A faster decreasing rate of PL intensity with 50 meV thermal activation energy is related to the increase in nonradoative recombination centres as the temperature increases. The temperature dependence of the relative intensities of the GaN band edge emission with respect to the YL (I_{BE}/I_{YL}) is also shown in figure 10. This ratio decreases with temperature and becomes less than 1 at room temperature indicating that the defect density in this sample is most probably due to the intensive diffusion of Si impurities from the Si substrate to the GaN epilayer.

4. Conclusions

In this study, the influence of the HT-AlN buffer layer thickness in the range from 300 to 500 nm and the AlGaN buffer layer thickness in the range from 700 to 950 nm on the GaN layer was investigated. Single crystalline GaN films were successfully grown on Si(1 1 1) substrates by MOCVD. The thicknesses of the GaN epitaxial layers exceeded 2.6 μm. The evolution of the surface morphology of GaN films as a function of the HT-AlN thickness was investigated. Crack-free flat GaN films were obtained with a 400 nm HT-AlN layer. Nearly crack-free GaN epitaxial layers were achieved by introducing step-graded AlGaN intermediate layers on optimized HT-AlN/Si(1 1 1) templates. The crystalline quality and morphology of the GaN layers significantly improved after the insertion of step-graded AlGaN layers. We found that stress relaxation due to the step-graded AlGaN layers was also dependent on the layer thickness. The step-graded AlGaN layers were grown to a total thickness of 700 nm. The edge and screw dislocation density changed with the HT-AlN layer thickness and the AlGaN intermediate layer thickness. For sample B, with a 400 nm HT-AlN template layer and a 700 nm AlGaN intermediate layer thickness, minimum dislocation densities were obtained.

At room temperature, the samples show a strong PL emission band between 3.387 and 3.394 eV due to the near-band edge emission from wurtzite GaN. The FWHMs of the band edge emission were within the range 58–62 meV. The small FWHM values of the PL emission peaks also indicate high-quality w-GaN material. The FWHMs of the near-band edge emission peak were 58 meV for sample B that was grown with a 700 nm AlGaN layer and a 400 nm HT-AlN layer which has the best optical property of all the samples.

Acknowledgments

This work is supported by the European Union under the projects EU-METAMORPHOSE, EU-PHOREMOST,

EU-PHOME, EU-ECONAM and TUBITAK under Project Numbers 105E066, 105A005, 106E198, 106A017. One of the authors (EO) also acknowledges the partial support from the Turkish Academy of Sciences.

References

[1] Pal S and Jacob C 2004 *Bull. Mater. Sci.* **27** 501
[2] Krost A and Dadgar A 2002 *Phys. Status. Solidi* a **194** 361
[3] Krost A and Dadgar A 2002 *Mater. Sci. Eng.* B **93** 77
[4] Nikishin S A, Faleev N N, Antipov G, Francoeur S, Grave de Peralta L, Seryogin G A, Temkin H, Prokofyeva T I, Holtz M and Chu S N G 1999 *Appl. Phys. Lett.* **75** 2073
[5] Gokkavas M, Butun S, Tut T, Biyikli N and Ozbay E 2007 *Photon. Nanostruct.* **5** 53
[6] Butun B, Cesario J, Enoch S, Quidant R and Ozbay E 2007 *Photon. Nanostruct.* **5** 86
[7] Yu H, Ozturk K M, Ozcelik S and Ozbay E 2006 *J. Cryst. Growth* **293** 273
[8] Amano H, Iwaya M, Hayashi N, Kashima T, Katsuragawa M, Takeuchi T, Wetzel C and Akasaki I 1999 *J. Nitride Semicond. Res.* **4S1** G10.1
[9] Yu J W, Lin H C, Feng Z C, Wang L S, Tripaty S and Chua S J 2006 *Thin Solid Films* **498** 108
[10] Kim M-H, Do Y-G, Kang H C, Noh D Y and Park S-J 2001 *Appl. Phys. Lett.* **79** 2713
[11] Ishikawa H, Zhao G Y, Nakada N, Egawa T, Soga T, Jimbo T and Umeno M 1999 *Phys. Stat. Sol.* (a) **176** 599
[12] Able A, Wegscheider W, Engl K and Zweck J 2005 *J. Cryst. Growth* **276** 415
[13] Cheng K, Leys M, Degroote S, Van Daele B, Boeykens S, Derluyn J, Germain M, Van Tendeloo G, Engelen J and Borghs G 2006 *J. Electron. Mater.* **35** 592
[14] Raghavan S and Redwing J M 2005 *J. Appl. Phys.* **98** 023514
[15] Jang S-H and Lee C-R 2003 *J. Cryst. Growth* **253** 64
[16] Mastro M A, Eddy C R Jr, Gaskill D K, Bassim N D, Casey J, Rosenberg A, Holm R T, Henry R L and Twigg M E 2006 *J. Cryst. Growth* **287** 610
[17] Dadgar A, Bläsing J, Diez A, Alam A, Heuken M and Krost A 2000 *Japan. J. Appl. Phys.* **39** L1183
[18] Wu C-L, Chou L-J and Gwo S 2004 *Appl. Phys. Lett.* **85** 2071
[19] Hageman P R, Haffouz S, Kirilyuk V, Grzegorczyk A and Larsen P K 2001 *Phys. Status Solidi* a **188** 523
[20] Metzger T, Höppler R, Born E, Ambacher O, Stutzmann M, Stömmer R, Schuster M, Göbel H, Christiansen S, Albrecht M and Strunk H P 1998 *Phil. Mag.* A **77** 1013
[21] Heying B, Wu X H, Keller S, Li Y, Kapolnek D, Keller B P, DenBaars S P and Speck J S 1995 *Appl. Phys. Lett.* **68** 643
[22] Vickers M E, Kappers M J, Datta R, McAleese C, Smeeton T M, Rayment F D G and Humphreys C J 2005 *J. Phys. D: Appl. Phys.* **38** A99
[23] Weimann N G and Eastman L F 1998 *J. Appl. Phys.* **83** 3656
[24] Holy V, Kubena J, Abramof E, Lischka K, Pesek A and Koppensteiner E 1993 *J. Appl. Phys.* **74** 1736
[25] Srikant V, Speck J S and Clarke D R 1997 *J. Appl. Phys.* **82** 4286
[26] Zheng X H, Chen H, Yan Z B, Han Y J, Yu H B, Li D S, Huang Q and Zhou J M 2003 *J. Cryst. Growth* **255** 63
[27] Williamson G K and Hall W H 1953 *Acta Metall.* **1** 22
[28] Sun Y J, Brandt O and Ploog K H 2003 *J. Mater. Res.* **18** 1247
[29] Sasaki H, Kato S, Matsuda T, Sato Y, Iwami M and Yoshida S 2007 *J. Cryst. Growth* **298** 305
[30] Gay P, Hirsch P B and Kelly A 1953 *Acta Metall.* **1** 315
[31] Dunn C G and Koch E F 1957 *Acta Metall.* **5** 548
[32] Reshchikov M A, Huang D, Yun F, He L, Morkoç H, Reynolds D C, Park S S and Lee K Y 2001 *Appl. Phys. Lett.* **79** 3779
[33] Freitas J A Jr, Moore W J, Shanabrook B V, Braga G C B, Lee S K, Park S S and Han J Y 2002 *Phys. Rev.* B **66** 233311
[34] Calle F, Sanchez F J, Tijero J M G, Sanchez-Garcia M A, Calleja E and Beresford R 1997 *Semicond. Sci. Technol.* **12** 1396
[35] Tu L W, Lee Y C, Stocker D and Schubert E F 1998 *Phys. Rev.* B **58** 10696
[36] Reshchikov M A and Morkoç H 2005 *J. Appl. Phys.* **97** 061301
[37] Neugebauer J and Vande Walle C G 1996 *Appl. Phys. Lett.* **69** 503
[38] Mattila T and Nieminen R M 1997 *Phys. Rev.* B **55** 9571
[39] Zhang J X, Qu Y, Chen Y Z, Uddin A, Chen P and Chua S J 2007 *Thin Solid Films* **515** 4397
[40] Viswanath A K, Lee J I, Yu S, Kim D, Choi Y and Hong C H 1998 *J. Appl. Phys.* **84** 3848
[41] O'Neill M, Oestreich M, Ruhle W W and Ashenford D E 1993 *Phys. Rev.* B **48** 8980
[42] Dean P J 1967 *Phys. Rev.* B **157** 655
[43] Rinaldi R, Antonaci S, Anni M, Lomascolo M, Cingolani R, Botchkarev A and Morkoc H 1999 *Phys. Status Solidi* b **216** 701
[44] Gangopadhyay S, Schmidt T and Falta J 2006 *Phys. Status Solidi* b **243** 1416
[45] Brazel E G, Chin M A and Narayanamurti V 1999 *Appl. Phys. Lett.* **74** 2367
[46] Zheng L X, Xie M H, Seutter S M, Cheung S H and Tong S Y 2000 *Phys. Rev. Lett.* **85** 2352